International Research Journal of Engineering and Technology (IRJET) e-ISSN: 2395-0056
Volume: 07 Issue: 06 | June 2020 www.irjet.net p-ISSN: 2395-0072

FUSION OF DIFFERENT MEDICAL SENSOR USING LOCAL LAPLACIAN PYRAMID TRANSFORM

K Rajesh[1], R Santhosh kumar[2], T Prasanth[3], N Naveen kumar[4]

[1]Assistant Professor, ECE Department, SSMIET, Dindigul, Tamil Nadu, India
[2,3,4]Under graduate student, ECE Department, SSMIET, Dindigul, Tamil Nadu, India

---

Abstract - *The Objective of project is to enhance the quality of medical sensor images for human perception and computerized image processing. The major anxiety about different medical sensor images is not providing comprehensive and accurate information. So this project aims to overcome the problems mentioned above by introducing local Laplacian pyramid transform (LLP) and adaptive cloud model (ACM). The project is classified into three groups. First, the input images like MRI and PET are decomposed into various levels using F-LLP. Second, fusion of two different approximate images is involved using ACM. Finally, reconstruction of original image will be performed by I-LLP.*

The assessment of medical image quality will be performed by different parameters like RMSE, PSNR, SD, MI and Entropy, cross entropy

***Key Words*: local laplacian pyramid transform, adaptive cloud model, image fusion.**

1. INTRODUCTION

MULTIMODAL sensor medical image fusion is the process of merging multiple medical images from a single imaging sensing modality or multiple imaging sensor modalities with limitation information, such as low spatial resolution or lack of functional information. Multimodal sensor medical images are roughly divided into two groups: anatomical images and functional images. Anatomical images (such as magnetic resonance imaging (MRI) and computed Tomography (CT)) provide high-spatial-resolution anatomical morphology of organs, but they cannot represent functional changes in the organs. On the other hand, functional images (such as positron emission tomography (PET) and single photon emission computed tomography (SPECT)) can obtain information about the metabolism of organs. Owing to their low resolution, functional images cannot display anatomical details of organs and lesions. To overcome the defects of various imaging techniques, multimodal sensor medical image fusion methods have been proposed to construct a fused image including both anatomical and functional information.

1.1. Pyramid Transformation

The basic idea is to construct the pyramid transform of the fused image from the pyramid transforms of the source images and then fused image is obtained by taking inverse pyramid transform. Here are some advantages of pyramid transform:

1. It can provide information on the sharp contrast changes and human visual system is especially sensitive to these sharp contrast changes.
2. It can provide both spatial and frequency domain localization Several types of pyramid decomposition are used or developed for image fusion such as

- Laplacian Pyramid
- Ratio of low pass pyramid
- Gradient Pyramid

A Laplacian Pyramid Image pyramid is a multiresolution analysis model. The Laplacian Pyramid implements a pattern selective approaches to image fusion, so that the composite image is constructed not a pixel at a time.. The basic idea is to perform a pyramid decomposition on each source image then integrate all these decomposition to form a composite representation and finally reconstruct the fused image by performing an inverse pyramid transform. Schematic diagram of the Laplacian Pyramid fusion method is shown in figure

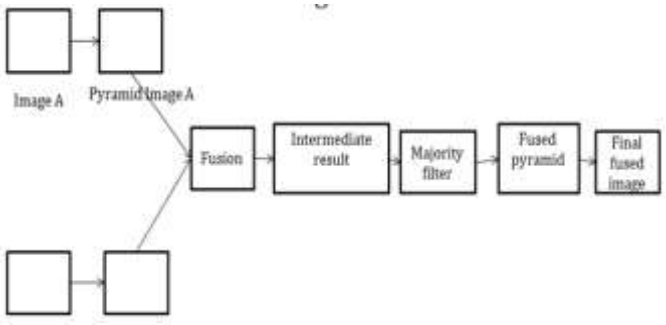

Laplacian Pyramid used several modes of combination such as selection or averaging. In the first one the combination process selects the component pattern from the source and copies it to the composite pyramid, while discarding the fewer patterns. In the second one, the process averages the sources patterns.

1.2. Wavelet Transform

The wavelet transform has become a very useful tool for image fusion. The wavelet based approach is appropriate for performing fusion takes for the following reasons 1. It is a multiscale (multiresolution) approach well suited to manage the different image resolutions. 2. The discrete wavelet transform allows the image decomposition in different kinds of coefficients preserving the image decomposition 3. Such coefficients coming from different images can be appropriately combined to obtain new coefficients so that the information in the original images is collected appropriately. 4. Once the coefficients are merged, the final fused image is achieved through the inverse discrete wavelets transform (IDWT), where the information in the merged coefficients is also preserved. The key step in image fusion based on wavelets is that of coefficients combination in order to obtain the best quality in the fused image. This can be achieved by set of strategies.

Illustrates two diagrams for g

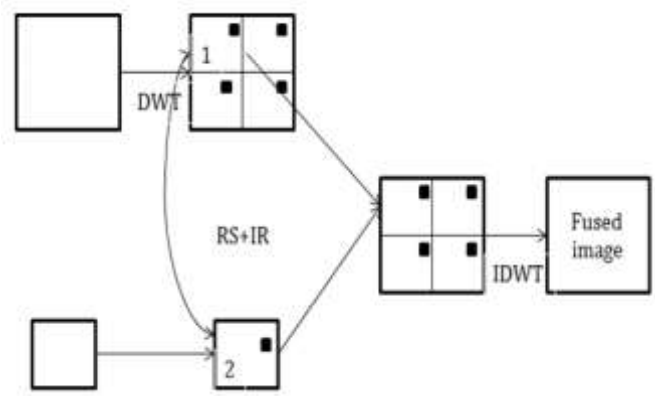

eneric MSD approaches. In the source images must have identical spatial resolutions. Hence, if their resolutions are different, an image resampling (RS) followed by an image registration (IR) strategies are previously required. The DWT is applied to both images and a decomposition of each original image is achieved. Only coefficients of the same level and representation are to be fused, so that the fused multiscale coefficients can be obtained. Once the fused multiscale is obtained, through the IDWT, the final fused image is achieved. There are two sources images with different resolution levels, the DWT is only applied to the image with the higher spatial resolution and then obtain a multiscale image representation for such image. Here only a unique type of coefficients belonging to the multiscale representation of the higher-resolution image and the original pixels of the smaller image are to be fused. A fused multiscale representation is obtained and as before, through the IDWT the final fused image is achieved.

1.3. Problems in Existing technique

Pyramid transform

1) Pyramid transform-based fusion methods were developed from the Gaussian pyramid transform.
2) Pyramid transform-based image fusion methods fail to capture directional information by multiscale image representation.

Discrete wavelet transforms (DWT), contourlet transform (CT), and shearlet transform (ST)

1) Provide a framework to capture the input images using multiscale and multidirectional representations.
2) The fused images are blurred with low contrast
3) The saliency features are sensitive to shift and noise.

2.1. BRIEF INTRODUCTION OF THE LOCAL LAPLACIAN PYRAMID

LP has been applied to fuse medical images with different modalities at multiple scales. However, the LP-based fusion method introduces artificial edges and halos. To overcome this limitation, LLP was proposed owing to its advantages of simplicity and flexibility. In theory, LLP is an edge-aware filter based on LP. It assumes that the filtering output O is constructed by the computation of a new LP for the intermediate image coefficients Si[I′] at each scale using the function

O = collapse (Si [I (v)])

For each coefficient I(v) = (x,y,i), we generate a new coefficient I′(v) by applying a point wise remapping function,

$$I'(V) = \begin{cases} g + sign(v-g)\sigma_r \left(\frac{|v-g|}{\sigma_r}\right)^{\alpha}, if\ |v-g| \le \sigma_r \\ g + sign(v-g)(\beta(|v-g|-\sigma_r)+\sigma_r), else, \end{cases}$$

Where x, y represent the pixel coordinate in horizontal and vertical orientations, respectively; i represents the level of the pyramid; v is the pixel value at position (x, y); and g is the image value resulting from the Gaussian pyramid. LLP has three free parameters: (1) the intensity threshold σr acts as the boundary for differentiating edge information from detail information, (2) the detail factor α controls the amount of detail enhancement ($0 \le \alpha < 1$) or detail smoothing, and (3) the ranging factor β controls the range compression ($0 \le \beta < 1$) or range expansion ($\beta > 1$). Moreover, for the color input image, the filtering output is obtained using LLP on red, green, and blue (RGB) channels of the input image. When β = 1, LLP has evolved into a detail manipulation filter.

2.2. ACM Scheme for Approximate Images

The approximate post-LLP image contains the pixel value distribution of the input medical images and reflects the anatomical and functional information of the brain. To preserve much more information of the approximate

images, the fused approximate image is constructed using the ACM scheme. The ACM model of the image could be characterized by three features : expectation (Ex), entropy (En), and hyper entropy (He). In the triple (Ex, En, He), Ex is a measure of the basic certainty for the qualitative concept and reflects the average level of theory domain. En is a measure of the uncertainty of the qualitative concept and reflects the degree of dispersion of cloud droplets. He is a measure of the uncertainty of entropy and reflects the thickness of the cloud model. The basic steps of the ACM scheme are described by Algorithm 2. Algorithm 2 includes three main steps: histogram fitting, ACM generation, and cloud reasoning rules.

In the first step (histogram fitting), for the input image of$G_{I_A}^L$ and $G_{I_B}^L$, the histogram of each image is calculated. The differential of the fitted histograms of images $G_{I_A}^L$and $G_{I_B}^L$is obtained by using a high-order spline function to fit each histogram and select valley points from the first-order derivative f′(x). The pixel values of the approximate images $G_{I_A}^L$ and $G_{I_B}^L$, presented by the gray histogram mainly range from 0 to 250. The larger value of the pixel corresponds to the detail information of anatomical and functional images. The peak point in the gray histogram for image $G_{I_B}^L$, indicated by the black arrow, is completely preserved in the fitted curve for image $G_{I_B}^L$, indicated by the red arrow. At the second step (ACM generation), according to the analysis of the gray histogram, we divide the pixel value distribution into p intervals using valley points. We dispose of some obscure valley points to facilitate the division of the intervals. Supposed the generated number of valleys is denoted as {k1, k2, ..., kp} in which 0∼ k1 is the first interval, k1 ∼ k2 is the second interval, ... , and kp ∼ k255 is the p-th interval. For gray values of each interval (xi, i=1, 2, ..., n), the multistep backward cloud transformation algorithm [21] is applied to obtain the feature triple (Ex, En, He). As shown in Fig. 4(d1) and (d2), four cloud models and three cloud models are generated for the approximate images using the forward cloud generator, respectively. Finally (cloud reasoning rules),

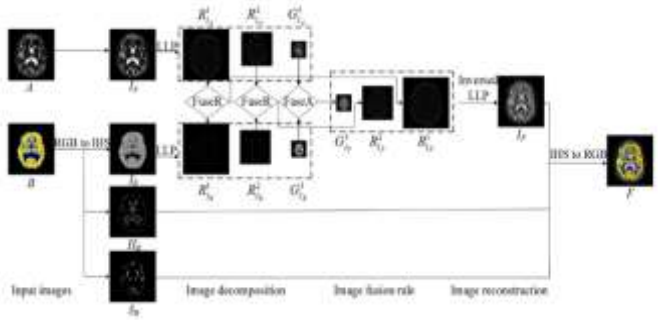

Fig:-2.1 Schematic diagram of the proposed fusion framework. Fuse R denotes the salience match measure rule for residual images, Fuse A denotes the adaptive cloud model scheme for approximate images

The input approximate images $G_{I_A}^L$ and $G_{I_B}^L$ are supposed to generate n1 and n2 cloud models, respectively. Pixel values of image $G_{I_A}^L$ stimulate the X condition cloud generator to generate a set of membership values. Averages of membership values in n1 cloud models of the approximate image $G_{I_A}^L$are denoted as μ11, μ12, L, μ1n1; similarly, averages of approximate image $G_{I_B}^L$are denoted as μ21, μ22, L, μ2n2. For a set of pixel values of approximate images $G_{I_A}^L$ and $G_{I_B}^L$ a two-dimensional cloud be constructed by the "multiplication algorithm" to achieve the process of μ1i × μ2j = μx. Let μ1 = μ11 × μ21; μ2 = μ11 × μ22; L, μn1×n2 = μ1n1 × μ2n2, and select the maximal value denoted as μmax.

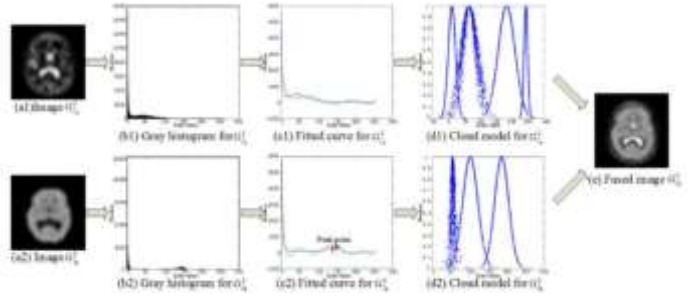

Fig:-2.2 Adaptive cloud model fusion process for GL IA and GL IB. (Red and black arrows denote the peak points of the fitted curve and gray histogram, respectively

The known maximal value μmax is the product of μ1i and μ2j. The average of the gray values in the variable μ1i, which stimulates the i-th cloud of approximate image $G_{I_A}^L$, is denoted as $\underset{X_I}{\rightarrow}$. The average of the gray values in the variable μ2j,which stimulates the j-th cloud of approximate image $G_{I_B}^L$is denoted as xj. The pixel value in the fused image $G_{I_F}^L$is the larger value between the average values xi and xj. As shown in Fig. 4(e), the maximal average value is chosen as the pixel value in the fused approximate image $G_{I_F}^L$.

2.3. Salience Match Measure for Residual

Images the human visual system has higher sensitivity to changes in the local detail information. Therefore, saliency match measure is applied to the fused residual images. Let$S_{R_I}^i(R_I = R_{I_A} or\ R_{I_B})$) be the salience measure for the residual images R_I^i and $R_{I_B}^i$ and w be the local window with size 3 × 3. The salience match measure is defined as follows. First, the saliency feature is calculated by

$$S_{R_I}^i(x,y) = \sum_{\Delta n \in w} \left| R_I^i(X + \Delta n, y + \Delta n) \right|^2$$

Second, the parameter M reflects the resemblance between $R_{I_A}^i$and $R_{I_B}^i$, used for quantifying the degree of similarity between the sources. The match measure M is defined as follows, where eps is a function in MATLAB.

$$M = \frac{2 \times \sum_{\Delta n \in w} \left| R_{I_A}^i(X + \Delta n, y + \Delta n) \right|^2}{S_{R_{I_A}}^{\ i}(x,y) + S_{R_{I_A}}^{\ i}(x,y) + eps}$$

$$\begin{cases} w_A = \frac{1}{2} - \frac{1}{2}\left(\frac{1-M}{1-\alpha}\right) & if\ M \geq \beta; \\ w_A = \begin{cases} 1, & S_{R_{I_A}}^{i} > S_{R_{I_B}}^{i}; \\ 0, & otherwise; \end{cases} & otherwise; \end{cases}$$

After many experiments, the value of threshold β is set as 0.75. Finally, the fused residual image is obtained using the weights via the salience match measure
$R_{I_F}^i = w_A R_{I_A}^i + w_B R_{I_B}^i$, Where $w_B = 1 - w_A$

3.1. Experimental Setup

To evaluate the quality of the proposed method, the testing dataset includes high-spatial-resolution MRI images shown in gray and low-spatial-resolution PET and SPECT images shown in pseudo-color. The testing medical images are co-registered. Furthermore, the testing medical imaging data have a resolution size of 256 _ 256. From the input source images in the figures, it can be noted that the MRI image captures the anatomical structural information of the human brain. In contrast, the PET and SPECT images reflect the blood flow changes in apparent shape acquisition. The quality metric for image fusion is a pertinent quality assessment tool to evaluate the visual quality degradation of images suffering from various distortions during the fusion procedure.

The metric visual information fidelity (*VIF*) [32] attempts to compute the loss of contrast information between the input and the fused images. The metric gradient-based index (*QAB=F*) is used to evaluate the edge information transferred from the input image to the fused image. The metric difference of entropy (*DEN*) [9] is used to compute the loss of the entropy information between the input image and the fused image. The metrics *VIF*, *QAB=F*, and *DEN* are among the full-reference image quality assessment tools. The metric natural image quality evaluator (*NIQE*), considered as no-reference image quality metrics, is applied to predict the distorted information with blind distortion types [34]. Interested readers can refer to these references on how to compute them.

3.2. Comparisons of LP and LLP

To demonstrate the advantages of the new image decomposition and reconstruction scheme, LLP is compared with LP this subsection. After many experiments, the parameters of LLP are set to _r = 0.3, _ = 0.25, _ = 1, and l = 4. The LLP and LP methods contain the same image fusion rule MAX, in which the fused approximate image is the average value of the approximate images and the fused residual image is the absolute value of the larger residual image. Fig. 5 displays the input images and the fused images obtained by the LP and LLP methods. Compared with the LP method shown in Fig. 5(c1) and (c2), the proposed LLP method, used as the new image decomposition and reconstruction scheme, introduces high-contrast detail information, as shown in Fig. 5(d1) and (d2). Moreover, in Table 2, the LLP method obtains higher values in terms of the metric *VIF*. This means that the LLP method has corrupted more contrast information from the inputs. The LLP method uses the threshold _r to distinguish edge from detail information [13]. The fused image obtained using the LLP method produces enhanced detail information.

First, the image Laplacian coefficient $I(v)$ is regarded as the detail information if the absolute differential value between the input image coefficient v and the input image Gaussian coefficient g is less than _r. If the detail parameter _ is less than 1, the new output detail Laplacian coefficient $I'(v)$ is greater than the input detail Laplacian coefficient $I(v)$.

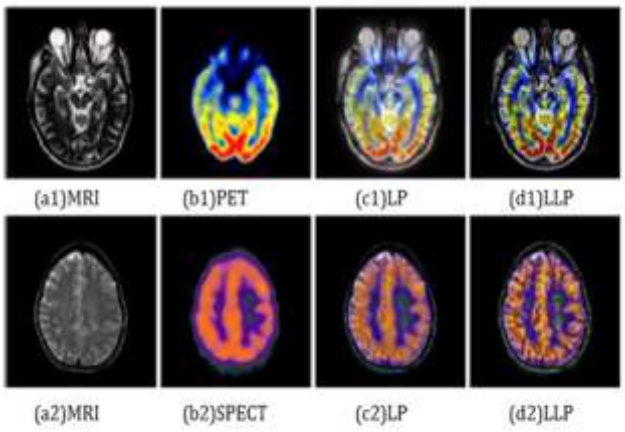

Fig:-3.1 Comparison of LP and LLP on two pairs of multimodal Sensor medical images

3.3. Comparisons of ACM and Different Fusion Rules

To verify the effective performance of the ACM method used as the fusion rule of the approximate image decomposed by the LLP method, Fig. 6 and Table III show both subjective and objective evaluations of image fusion results on noise free images using MAX, sparse representation (SR) [35], spatial frequency (SF) [36], deep convolutional neural networks (CNN) [37], and ACM-based fusion rules. The fused image corresponds to the maximum of the absolute pixel values in the input images using the MAX-based fusion rule. The SR based fusion rule using the trained feature helps reconstruct each pixel of the fused image. The SF-based fusion rule takes the spatial resolution in horizontal and vertical directions as the weights of the input images. The CNN-based fusion rule constructs the decision map of the fused image by the CNN feature.

TABLE:- 3.1 OBJECTIVE EVALUATION OF THE FUSED IMAGES USING LP AND LLP

VIF			VIF		
MRI-PET	LP	0.2116	MRI-SPECT	LP	0.3192
	LLP	**0.2512**		**LLP**	**0.3202**

Fig displays two sets of noise-free medical image testing data for the fusion of MRI and PET images and the fusion of MRI and SPECT images. In the experimental setup, the scale *l* is set to 4. To compare the fused result using the LLP+ACM method with the fused result using the LLP+MAX, LLP+SR,

TABLE:-3.2 OBJECTIVE EVALUATION OF THE FUSED IMAGES WITH ACM AND DIFFERENT FUSION RULES INTEGRATED WITH LLP

VIF			VIF		
MRI-PET	LLP+ MAX	0.3131	**MRI-SPECT**	LLP+ MAX	0.4121
	LLP+ SR	0.3071		LLP+ SR	0.4075
	LLP+ SF	0.3139		LLP+ SF	0.4512
	LLP+ CNN	0.1534		LLP+ CNN	0.1907
	LLP+ ACM	**0.5793**		**LLP+ ACM**	**0.5373**

LLP+SF, and LLP+CNN methods, it can be concluded that the ACM-based image fusion rule generates the high-contrast intensity detail because ACM uses the fitted curve to represent the image detail information by the capture of the valley point of the fitted curve for the approximate images. However, the CNN-based image fusion rule introduces arte facts around the boundaries of the brain. The trained model in the CNN-based image fusion rule is not helpful to preserve the important features of the input medical images. On the other hand, the quantitative evaluation using the metric *VIF* is given in Table II.

From Table II, the proposed ACM-based image fusion rule performs better than the MAX, SR, SF, and CNN-based image fusion rules

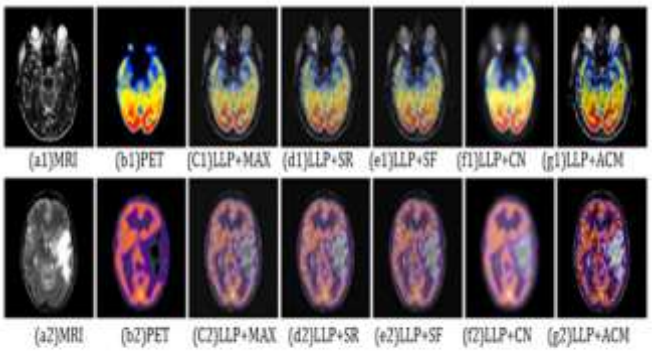

Fig:-3.2 Image fusion on noise-free using different image fusion rules

3.4. Overall Comparisons of LLP+ACM and State-of-the-art Methods

This subsection gives the overall comparison between LLP+ACM and seven state-of-the-art fusion methods. The NSCT, ST, GIHS, image fusion with guided filtering (GFF) [38], and image fusion using local extrema scheme (LES) [39] methods are related to medical image fusion. The boosting Laplacian pyramid (BLP) method [27] is used to boost the details with better color appearance and more texture details in the field of multi-exposure image fusion. Image fusion using the gradient transfer (GTF) method [40] using total variation preserves the gradients with large magnitude for the fusion of infrared and visible images. Fig exhibit the fusion results on noise-free images for the fusion of MRI and PET images and of MRI and SPECT images, respectively. Fig. shows the input MRI image, the input PET image, and the fusion results obtained using the NSCT, ST, GIHS, GFF, LES, GTF, BLP, and LLP+ACM methods. The NSCT, GIHS, and GFF methods combine the structural and functional information of the inputs. Nevertheless, the detail information is not enhanced in the results, shown in Fig. (c), (e), and (f).The visual result on the last line of Fig. (e1) displays the zoomed region of the square box shown by the red color in the result image obtained using the GIHS method. From Fig. 7 (e1), it can be concluded that the detail is not enhanced. The white matter of the human brain represents changes in metastatic bronchogenic cancer

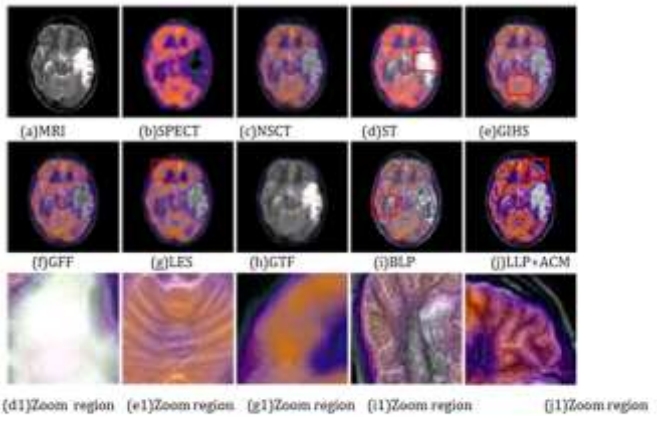

Fig-3.3 Image fusion results on noise-free images for fusion of MRI and SPECT images

Using the MRI image, shown in Fig. (a). The results using the ST, GTF, and LLP+ACM fusion methods perform better in preserving the white matter of the input MRI image. In contrast to the proposed LLP+ACM method, the ST method fails to extract the black hole in the center of the white matter, shown in Fig. (d) and (d1). In addition, the GTF method preserves nothing but the structural information from the input MRI image. By carefully observing Figs. 7-8, the LLP+ACM method introduces both enhanced structural detail information from the input anatomical medical imaging data and enhanced color information from the input functional medical imaging data. Table presents the quantitative evaluation of noise-free images for the fusion of MRI and PET images and of MRI and SPECT images. The higher the *VIF* and *QAB=F* metrics, the better the method performs. From Table, the LLP+ACM method obtains the largest values in terms of the *VIF* and *QAB=F* metrics compared with the other fusion methods. For the *DEN* metric, the fusion of MRI and PET images contains most of the information from the input images. For the *NIQE* metric, the LLP+ACM method for the fusion of MRI and SPECT images performs better than that for the fusion of MRI and PET images.

TABLE:-3.3 QUANTITATIVE EVALUATION OF NOISE-FREE IMAGES

		VIF	***QAB=F***	**DEN**	**NIQE**
MRI-PET	NSCT	0.2072	*0.1600*	0.6302	7.0992
	ST	0.3613	*0.2196*	1.5209	5.5704
	GIHS	0.3517	*0.2399*	0.4499	5.5463
	GFF	0.3353	*0.2392*	0.5215	**5.5262**
	LES	0.1592	*0.1423*	0.4408	8.3993
	GTF	0.1919	*0.1387*	0.5227	7.1711
	BLP	0.4991	*0.2266*	0.6376	8.4561
	LLP+ ACM	**0.5442**	***0.2527***	**0.3791**	6.1074
MRISPECT	NSCT	0.2070	*0.1809*	0.5555	8.0808
	ST	0.3734	*0.2506*	1.0671	6.5733
	GIHS	0.3737	*0.2645*	0.4846	6.0473
	GFF	0.3112	*0.2532*	0.4819	6.4506
	LES	0.1835	*0.1891*	0.4768	7.8199
	GTF	0.2095	*0.1792*	**0.4023**	12.9025
	BLP	0.3850	*0.2410*	0.4763	7.3451
	LLP+ ACM	**0.5249**	***0.2968***	0.9203	**5.6270**

TABLE:-3.4 COMPARISON OF COMPUTATIONAL TIMES OF DIFFERENT METHODS (S)

NSCT	**ST**	**GIHS**	**GFF**	**LES**	**GTF**	**BLP**	**LLP+ACM**
22.87	140	0.05	0.32	35.89	6.10	115.19	3964.19

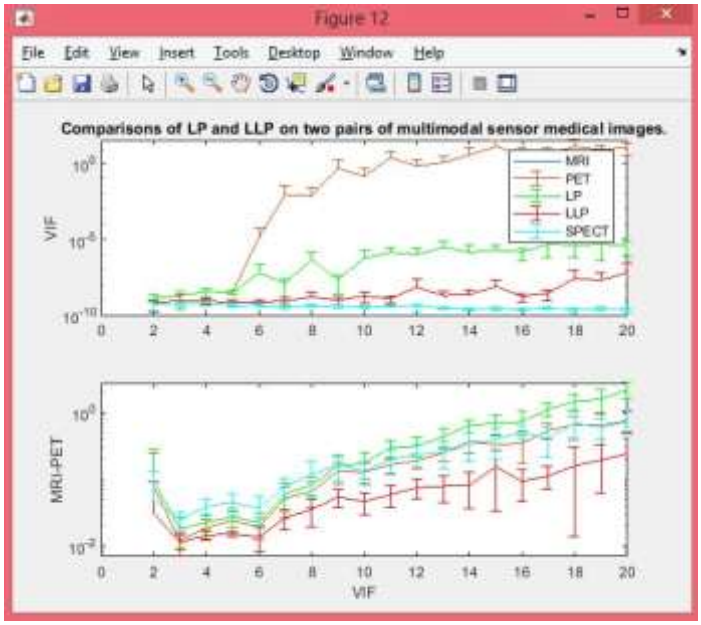

Fig:-3.4 comaparisons of LP and LLP

4. Conclusion:

In this paper, we propose a new multimodal sensor medical image fusion framework, LLP+ACM. The merits of the LLP+ACM method include the following: (1) The LLP method, adopted for multi scale image representation, helps increase the contrast of details while removing halo artifacts. (2) ACM is used as the image fusion rule of the approximate image, which could better reflect the adaptability and intelligence of multimodal sensor medical image fusion. Extensive empirical studies show that the ACM method helps preserve both color and textural details. However, the LLP+ACM method has some drawbacks.

4. FUTURE WORK:

Fully convolutional networks are used to train the input medical images for detecting the specific noise. The trained data are then used to reconstruct the fused image to reduce noise while preserving details. Instead of using the pixel-by-pixel method, the patch-by-patch method will help reconstruct the final fused image using inversed LLP.

5. ACKNOWLEDGEMENTS

First and foremost, we would like to express our deep sense of gratitude to our most honorable Chairman and Management Trustee **Mr.P.S.Velusamy**, our honorable secretary and Management Trustee **Mr.C.Kandaswamy**, our beloved Executive Directors and Management Trustee **Mr.K.Shanmugavel** and **Mr.K.Sivaraj** of SSM Institute of Engineering and Technology for providing us with necessary facilities during the course of study. We feel immensely pleased to express our sincere thanks to our Principal **Dr.D.Senthil kumaran** for encouragement and support extended by them. We express our sincere thanks to our guide **Mr.K.Rajesh,** for his guidance throughout our project work. Also, we express our thanks to the faculty members of our Department, non-teaching staff members and my dear friends to their moral support, help and encouragement towards the successful completion of the project.

6. REFERENCES:

[1]J. Du, W. Li, and B. Xiao, "Anatomical-functional image fusion by information of interest in local laplacian filtering domain." IEEE Transactions on Image Processing A Publication of the IEEE Signal Processing Society, vol. PP, no. 99, pp. 1–1, 2017.

[2] S. Park, J. Jang, J. Kim et al., "Real-time triple-modal photoacoustic, ultrasound, and magnetic resonance fusion imaging of humans." IEEE Transactions on Medical Imaging, vol. 39, no. 9, pp. 1912–1921, 2017.

[3] J. Du, W. Li, K. Lu et al., "An overview of multi-modal medical image fusion," Neurocomputing, vol. 215, pp. 3–20, 2016.

[4] Y. Yang, Y. Que, S. Huang et al., "Multimodal sensor medical image fusion based on type-2 fuzzy logic in nsct domain," IEEE Sensors Journal, vol. 16, no. 10, pp. 3735–3745, 2016.

[5] J. Du, W. Li, B. Xiao et al., "Union laplacian pyramid with multiple features for medical image fusion," Neurocomputing, vol. 194, no. C, pp. 326–339, 2016.

[6] W. Wang, J. Shen, L. Shao et al., "Correspondence driven saliency transfer," IEEE Transactions on Image Processing, vol. 25, no. 11, pp. 5025–5034, 2016.

[7] V. Bhateja, H. Patel, A. Krishn et al., "Multimodal medical image sensor fusion framework using cascade of wavelet and contourlet transform domains," IEEE Sensors Journal, vol. 15, no. 12, pp. 6783–6790, 2015.

[8] J.Shen, Y.Zhao, S.Yanetal. "Exposure fusion using boosting laplacian pyramid." IEEE Transactions on Cybernetics, vol. 44, no. 9, pp. 1579– 1590, 2014.

[9] B. Martifuster, O. Esteban, K. Thielemans et al., "Including anatomical and functional information in mc simulation of pet and spect brain studies. Brain-viset: a voxel-based iterative method." IEEE Transactions on Medical Imaging, vol. 33, no. 10, pp. 1931–1938, 2014.

[10] R.Shen, I.Cheng and A.Basu, "Cross-scale coefficient selection for volumetric medical image fusion." IEEE Transactions on Biomedical Engineering, vol. 60, no. 4, pp. 1069–79, 2013.